Peer-reviewed version available at *Micromachines* **2020**, *11*, 270; doi:10.3390/mi11030270

Type of the Paper (Article)

High-Sensitivity Detection of IgG Operating Near the Dispersion Turning Point in Tapered Two-Mode Fibers

Bing Sun [1,2,3], and Yiping Wang [1,2,*]

[1] Guangdong and Hong Kong Joint Research Centre for Optical Fibre Sensors, College of Physics and Optoelectronic Engineering, Shenzhen University, Shenzhen 518060, China; graduate_sunbing@163.com
[2] Key Laboratory of Optoelectronic Devices and Systems of Ministry of Education and Guangdong Province, Shenzhen University, Shenzhen 518060, China
[3] graduate_sunbing@163.com
* Correspondence: ypwang@szu.edu.cn; Tel.: +86-0755-26066281

Abstract: Conventional method for monitoring the IgG levels suffered from some apparent problems such as long assay time, multistep processing, and high overall cost. An effective and suitable optical platform for label-free biosensing has been investigated by the implementation of antibody/antigen immunoassays. Thus, the ultrasensitive detection of IgG levels can be achieved by exploiting the dispersion turning point (DTP) existed in the tapered two-mode fibers (TTMFs) due to the sensitivity will reach ±∞ on either side of the DTP. Tracking the resonant wavelength shift it was found that the fabricated TTMF device exhibited limits of detection (LOD) down up to concentrations of 10 fg/mL of IgG in PBS solution. Such immunosensors based on the DTP have great significance on trace detection of IgG due to simple detection scheme, quick response time, and miniaturation.

Keywords: biosensor; optical fiber sensor; two-mode fiber; sensitivity

1. Introduction

Immunoglobulin G (IgG) is a short chain of amino acids connected by peptide bonds, and each molecule has 2 antigen binding, which it uses to protect using from invading organisms. IgG, which represents approximately 75% of serum antibodies in humans, is the most common type of antibody found in blood circulation. Clinically, the levels of IgG can be generally considered to be indicative of an individual's immune status to particular pathogens. Conventional method including enzyme linked immunesorbent assay (ELISA) is the gold standard method for monitoring the IgG levels due to its sensitivity and accuracy. However, it suffered from some apparent problems such as long assay time, multistep processing, high overall cost and require sophisticated instrumentation. Meanwhile the development of in-situ and real-time detection devices is an innovative field in applied research and healthcare diagnostics. Especially, label-free biosensors based optical fibers with high sensitivity for the recognition of low concentrations of analytes have become a research hotspot [1]. Among these optical fiber biosensors, they can be based on many constructions such as fiber gratings [2-4], special fibers [5-7], novel fibers with mechanical treatment [8-9] and so on. Furthermore, the advancement of nanotechnology plays an essential role in the field of biosensing benefited from advanced materials and nanostructures as transducer elements or reporters [10]. Chen Liu et al. explored graphene oxide nanosheets functionalized dual-peak long period grating based biosensor for immunosensing detection, and the limit of detection (LOD) is 0.05 mg/ml [11]. It's undeniable that the relative sensitivity and LOD are excellent due to the high RI sensitivities.

On other hands, one kind of microfiber working at the turning point can show infinite RI sensitivities. Luo et al. reported a high RI sensitivity of 10777.8 nm/RIU but the microfiber was

Peer-reviewed version available at Micromachines 2020, 11, 270; doi:10.3390/mi11030270

concentrated on the utilization of single-mode fiber configuration [12]. Similarly, researcher exploited optical microfiber coupler sensor working near the turning point of effective group index difference between the supermodes to achieve high RI sensitivity [13-16]. Among these, Zhou et at. demonstrated an ultrasensitive label-free optical microfiber coupler biosensor with diameter of 1.0 μm for detection of cardiac troponin I based on interference turning point effect. Experimental experience revealed that the fabrication and integration of such an optical microfiber coupler in a chamber was challenge [15]. In this study, a high-sensitivity biosensor based on a tapered two-mode fiber (TTMF) sandwiched between two SMFs has been experimentally demonstrated. Experimental results indicate that the RI sensitivity will also be significantly enhanced when it works around the dispersion turning point. Furthermore, this biosensor exhibits a sensitive response to IgG levels over the concentration range of 5-500 fg/mL in PBS buffer. Besides, a detection limit of 10 fg/mL in PBS buffer is obtained, which is a useful tool for practical application in clinical diagnosis. Moreover, the structure is easy to fabricate, highly stable, and easy to integrate with a plastic chamber.

2. Theoretical Analysis

A ring-core two mode fiber (TMF, http://www.yofc.com) has been employed, and the cross-section and index profile of the TMF can support fundamental (HE_{11}) modes and the second-order (HE_{21}) modes while the spatial profile of such modes is depicted in Fig. 1. Tapering the two mode fiber is recognized as a straight and efficient tool to achieve a uniform modal interference mainly involving with HE_{11} and HE_{21} modes. Thus, we propose a tapered two mode fiber (TTMF) based biosensor structure, which consists of an input SMF, a down-taper region, a TTMF section, an up-taper region, and an output SMF. We have to understand that the number of modes existed in the TTMF are determined by the diameter of TTMF (D_w) and the external surrounding (n_{ext}) [17], as a result, the section of TTMF needs to be sophisticatedly designed to develop a desired interferometer.

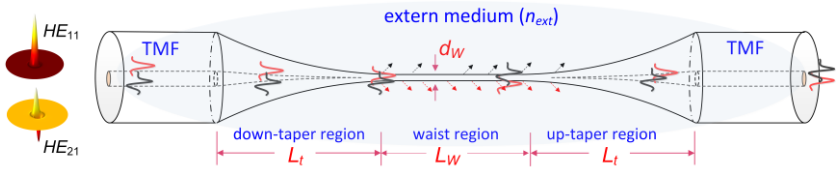

Figure 1. Schematic diagram of the sensor. Quasi adiabatic transition tapers provide continuous mode evolution from HE_{11} and HE_{21} modes when the two modes launched into the fiber are collected at the fiber output, respectively.

Also, owing to the cosine function of phase difference between the HE_{11} and HE_{21} modes, the evolution of the transmission spectra can be illustrated according to the two-mode interferometric theory as follows.

$$I = I_1 + I_2 + 2\sqrt{I_1 I_2}cos\ (\Phi) \tag{1}$$

where $\Phi = 2\pi\Delta n_{eff}L/\lambda$ is the phase difference between the HE_{11} and HE_{21} modes, Δn_{eff} is the effective RI difference of the HE_{11} and HE_{21} modes, L is the effective length of the taper, I_1 and I_2 are the intensities of the HE_{11} and HE_{21} modes, respectively. Thus, the interference dip (λ_m) can be defined.

$$\lambda_m = \Delta n_{eff}L/(m + 1/2),\ m \text{ is a positive integer} \tag{2}$$

Furthermore, the response of the transmission interference dip λ_m to external RI (n_{ext}) can be deduced through several mathematical treatment of Φ and then its relationship (i.e., S) can be expressed

$$S = \frac{d\lambda_m}{dn_{ext}} = \frac{1}{\Gamma}\frac{\lambda_m}{\Delta n_{eff}}\frac{d\Delta n_{eff}}{dn_{ext}} \tag{3}$$

where the determinative parameters of S are the wavelength λ_m, the RI-induced variation of index difference $d\Delta n_{eff}/dn_{ext}$, and the dispersion factor Γ ($1 - \lambda_m/\Delta n_{eff} \times d\Delta n_{eff}/d\lambda_m$). Furthermore, Γ and $d\Delta n_{eff}/dn_{ext}$ are dominated by the d_w and n_{ext}. Previously, we can conclude that the values of the dispersion factor Γ increase with the thinner microfiber [19]. It's interesting and meaningful that the

Peer-reviewed version available at Micromachines 2020, 11, 270; doi:10.3390/mi11030270

dispersion turning point (DTP) appears when the dispersion factor Γ approaches zero. According to Eq. (3), at the DTP, Γ approaches zero, and then the RI sensitivity is enhanced significantly to be ±∞.

3. Results

3.1 refractive index sensing

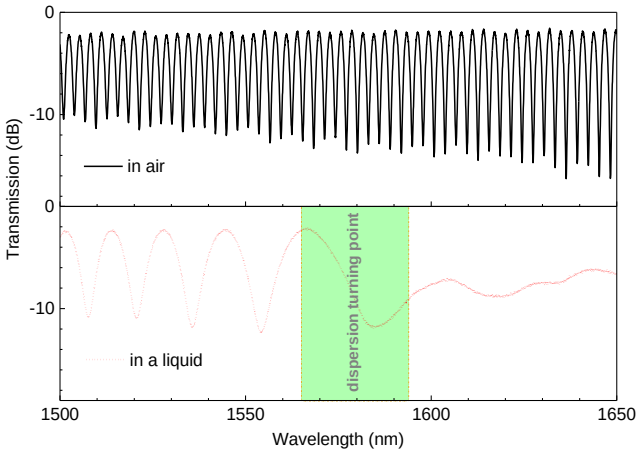

Figure 2. Variation of the interference spectra of the TMMF when immersed in air and a liquid.

Initially, we utilized the flame-brushing technique to fabricate the TTMF structure, where three stages assembled with electric motors, a hydrogen generator, and an oxyhydrogen torch were employed. And the taper sample can be fabricated through sophisticatedly defining parameters, i.e., the pulling speed, the hydrogen flow rate, and these can be found in the previous results [20]. Thus, we carry out experiments to investigate the spectral characteristics and the RI sensing capabilities of the TTMF. As illustrated in Fig.2(a), the transmission of a taper with a width of ~4.7 μm is produced by the flame-brushing technique while the length of the uniform waist and the tapered transition regions are ~7 mm and ~11 mm, respectively. It's obvious that the tapered TMF helps to establish a stable Φ, then leads to the interference status. Note that the DTP does not disappear in the given wavelength range when it's surrounded by air. By contrast, the corresponding spectrum shows evident changes when the structure is immersed into an index-matched liquid, thus the DTP appears around the wavelength of 1570 nm. We believe that the dispersion factor plays a dominate role in this phenomenon.

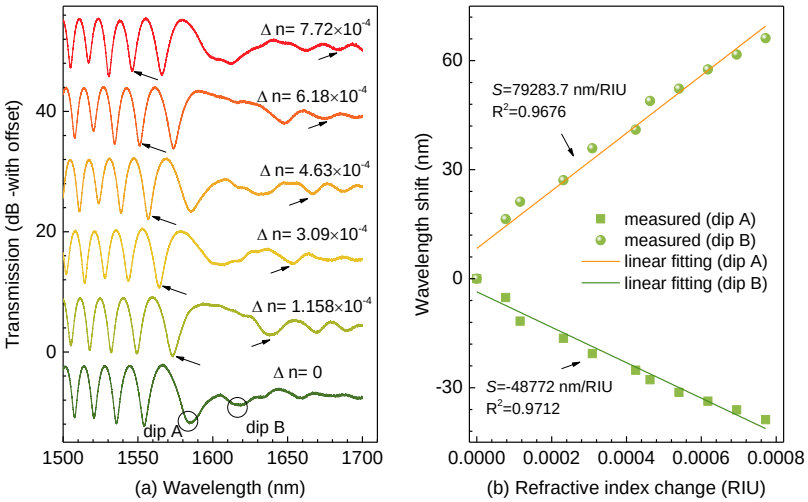

Figure 3. Variation of interferential spectra as the ambient refractive index. (b) Wavelength shifts of dips A and B versus ambient refractive index.

Peer-reviewed version available at Micromachines 2020, 11, 270; doi:10.3390/mi11030270

The abovementioned ultrasensitive characteristics have been also proposed [12-17], where minor refractive index variation can induce evident shift of the dip around the DTP. However, to induce minor refractive index change is challenge. In addition, it does cause uncertainty and then measurement error though various glycerol solution with different weight concentrations were prepared [20]. So in this experiment we induce minor refractive index change with different views. Initially, an index-matching liquid, which possesses a RI of 1.34 at 589.3 nm, and a thermal coefficient of dn_{fluid}/d_T=-3.38×10^{-4}/°C is employed, and then the TTMF is immersed into such liquid packaged in a flow cell. Next, we can precisely control the surrounding temperature by means of utilizing the flow cell into a high-precision column oven (LCO 102) with an accuracy of 0.1 °C. Also, a differential thermocouple (UNI-T UT320) is used to monitor the surrounding temperature. Besides, we need not take notice of the temperature cross-sensitivity of the TTMF as the thermal expansion of fused silica is of the order of 10^{-7}/°C. Accordingly, we establish a temperature control system to obtain the minor refractive index change during the experiment. Fig. 3(a) illustrates the transmission spectra shift with the ambient refractive index. The experimental results reveal that the resonant dip on the left side of the DTP shifts linearly toward a shorter wavelength, i.e. so-called 'blue' shift while the resonant dip on the right side of the DTP shows 'red' shift with increase of the ambient refractive index. It's easily understood that the increase of n_{ext} can normally generate a larger index increment for the HE_{21} mode than that for the HE_{11} mode, producing $d\Delta n_{eff}/dn_{ext}<0$. On the other hand, we have $\Gamma>0$ since the group velocity of the HE_{11} mode is larger than the HE_{21} mode on the left side of the DTP. Thereby a negative S is enabled, corresponding to a 'blue' shift (dip A) of wavelength with an increase of n_{ext} while the dip B shows the opposite trend. Furthermore, Fig. 3(b) presents sensitivities of the resonant dips closest to the DTP (dip A and dip B), which provides the highest sensitivity of -48772 nm/RIU and +79283.7 nm/RIU, respectively. More significantly, the resonant dips on both sides of the DTP shift to the opposite directions with the variations of the ambient refractive index. Thereby, an improved sensitivity of ~128055.7 nm/RIU is achieved, which is a competitive result compared to the state-of-the-art fiber-optic refractive index sensors.

3.2 Detection of IgG levels

3.2.1 Functionalization of biosensor

To further demonstrate the applicability and to improve upon the TTMF-based biosensor, we used it for the quantitative detection of IgG in PBS, and the biodetection process of which are depicted in Fig. 4. Prior to the functionalization we thoroughly cleansed the microfiber surface to remove any traces of glycerin, first with distilled water and then with methanol. Immediately the microfiber was cleaned with distilled water and then it was immersed in 0.1 M KOH solution for 10 min to create hydroxyl(-OH) groups on the surface. The surfaces were then washed with distilled water. Next the fiber biosensor surface was prepared by incubation for 30 min with 1 wt% poly (diallyldimethylammonium chloride) (PDDA, Mw: 200000-350000, 20 wt% in H_2O, purchased from Sigma-Aldrich). After cleaned with distilled water, the microfiber was immersed into 1 wt% poly poly acrylic acid solution (PAA, Mw: ~100000, 35 wt% in H_2O, purchased from Aldrich) to get final modification with individually spotted capture proteins. The surfaces were also washed with distilled water. Immobilization of biomolecules on device surface is an important step in the biosensor development. The covalent immobilization of anti-IgG on fiber surface might lead to improper orientation by masking antigen-binding sites. This shortcoming can be circumvented by using heterobifunctional cross-linkers of EDC/NHS combination. The microfiber was immersed into a mixture (1:1) of EDC and NHS in 0.01 M PBS buffer for 30 min. And then the sensor was washed thoroughly with the PBS. Subsequently, functionalized fiber was incubated with anti-IgG with concentration of 50 mg/L for 1 h to immobilize the antigen to fiber surface. Blocking to reduce subsequent non-specific binding was then performed by incubating the sensor with a blocking solution (3% BSA in PBS, pH 7.4) for 30 min. The biosensor chip was then washed with PBS for 5 min.

Peer-reviewed version available at Micromachines 2020, 11, 270; doi:10.3390/mi11030270

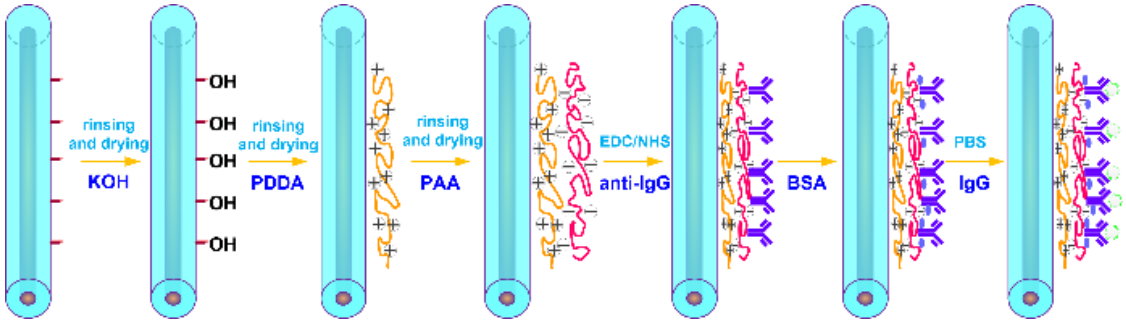

Figure 4. Procedure of PDDA and PAA modification for IgG immunoassay.

3.2.2 Experimental setup

The IgG and anti-IgG binding was performed by injecting and incubating 50 μL of IgG solutions for different concentrations with rinsing stages of the biosensor using PBS solution. The PBS rinse stage was used to establish the baseline associated to each increasing IgG concentration and to remove the unbound antigens from the previous solution. The experimental setup of the immunosensing performance characteristics is illustrated in Fig. 5. A broadband source (ASE) with a low polarization spectral range of 1250-1650 nm (www.optical-source.com) was used as the light source and its transmission spectra were monitored by an optical spectrum analyzer (OSA) with a minimum resolution of 0.02 nm in the involving spectral range. Moreover, the biosensor was embedded in a flow cell with the facilities of inserting and removing the biological sample, and both the ends of the flow cell were sealed with UV curable epoxy.

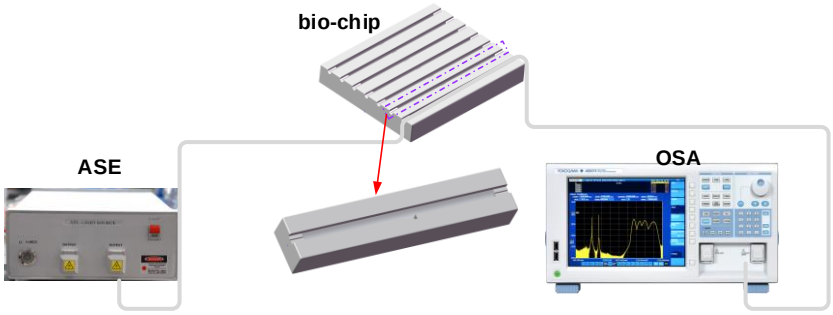

Figure 5. Experimental setup for the biosensing structure.

As illustrated in Fig. 6(a), we can easily notice that the DTP appears at around 1400 nm while we evaluate its immunosensing performance on the right side of the DTP as a wavelength shift in real time. Note that the interferometric spectra share the general envelope with that immersed into the index-matched liquid while induce several ripples across the interference. We notice that the polyelectrolyte layers immobilized onto the surface of the microfiber can lead to exciting higher-order modes, and then probably introduce multiple interference in the biosensor. Nevertheless, we can track the DTP region, further locate the resonant dip on the right side of the DTP though it isn't easy to be determined at first. However, the evident contrast of the resonant dip happens as the concentration is increased. Besides, it has to allow some experience for tracking the resonant dip. Furthermore, the spectra gradually show 'blue' shift when the IgG concentration is increased, the anti-IgG are gradually exhausted and the spectral shift reaches a plateau, i.e. for the IgG concentration of 500 fg/mL due to saturation effect which can be considered a complete antibody antigen procedure process. As a result, the shifts of the dip are fitting by rotational function with a high coefficient R^2, as show in Fig. 6(b).

Peer-reviewed version available at Micromachines 2020, 11, 270; doi:10.3390/mi11030270

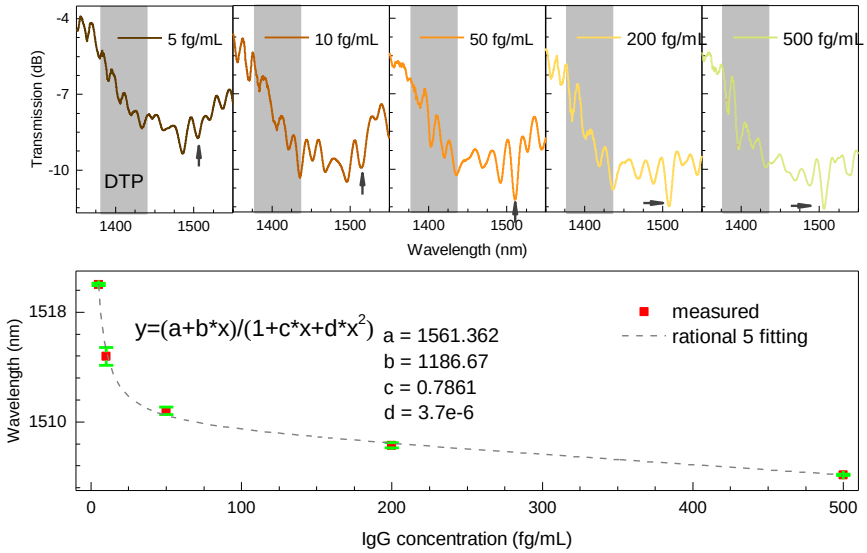

Figure 6. (a) Transmission spectral responses near the DTP, (b) Resonant shift with different concentrations of IgG.

3.2.3 Evaluation of antibody-antigen binding interaction

To further show the dynamic process, the real-time response to IgG with concentrations ranging from 5 fg/mL to 500 fg/mL have been obtained by continuously recording the interferometric dip near the DTP, which is shown in Fig. 7. We notice that the spectra hardly show any shift for an IgG concentration of 5 fg/mL as we believe such concentration is beyond the limit of detection of the proposed biosensor. However, the procedure procedure is intense for an IgG concentration of 10 fg/mL and robust, and a maximum wavelength shift of ~1 nm is recorded during this stage. Accordingly, we conclude that a limit of detection down up to concentrations of 10 fg/mL of IgG in PBS solution can be achieved and the concentration range is no more than 500 fg/mL.

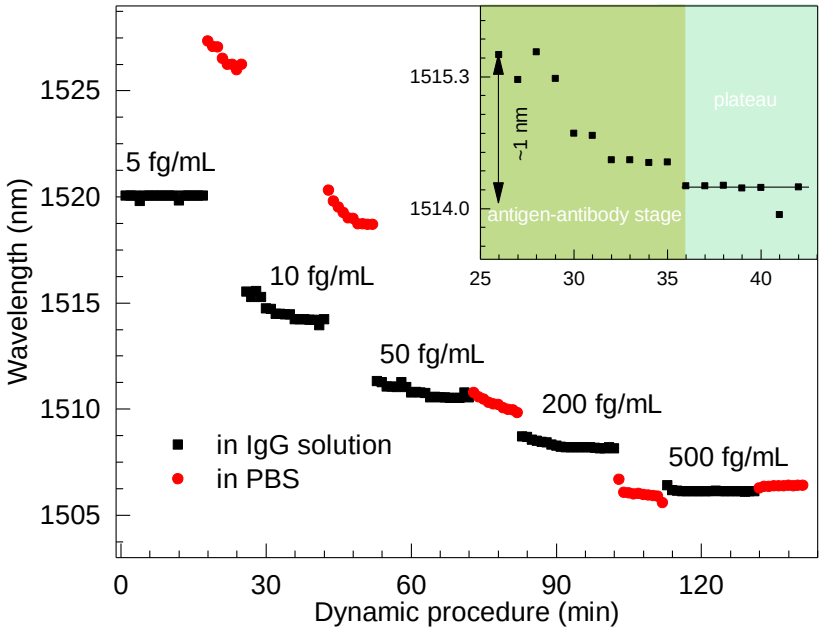

Figure 7. Spectral shift of the biosensor at different stages of IgG binding events.

Returning to the detection procedure with the concentration of 10 fg/mL of IgG, the dynamic procedure can be understood. Initially, the amounts of anti-IgG are rich and then it matches with that of IgG, and this can be illustrated in the enlarged window of Fig. 7. Thus, the procedure tends to be

Peer-reviewed version available at Micromachines 2020, 11, 270; doi:10.3390/mi11030270

stable as it's recorded within 20 minutes. So we can easily achieve the resonant dip while conclude the antibody-antigen procedure involves approximate 15 minutes. We also understand the detection of IgG is a challenging work and we try to clarify it in the future.

4. Conclusion

We have comprehensively investigated the temperature response of the TTMF. Utilizing the DTP, both ultrahigh refractive index sensitivities (with a negative sensitivity of of -48772 nm/RIU and a positive sensitivity of +79283.7 nm/RIU) have been experimentally demonstrated. Furthermore, relying on the excellent index sensing capability, an ultra-sensitive biosensor is also demonstrated. The proposed TTMF device exhibited limits of detection down up to concentrations of 10 fg/mL of IgG in PBS solution. Moreover, it is expected that this novel microfiber can serve as a necessary step towards potential applications for fast and accurate quantification of biomarker concentrations in clinical settings.

Acknowledgments: National Natural Science Foundation of China (61505119), National Postdoctoral Program for Innovative Talents (BX201600077), Brain Gain Foundation of Nanjing University of Posts and Telecommunications (NY215040), China Postdoctoral Science Foundation (2017M611877) and the Key Laboratory of Optoelectronic Devices and Systems of Ministry of Education and Guangdong Province (GD201706).

Author Contributions: For research articles with several authors, a short paragraph specifying their individual contributions must be provided. The following statements should be used "X.X. and Y.Y. conceived and designed the experiments; X.X. performed the experiments; X.X. and Y.Y. analyzed the data; W.W. contributed reagents/materials/analysis tools; Y.Y. wrote the paper." Authorship must be limited to those who have contributed substantially to the work reported.

Conflicts of Interest: The authors declare no conflict of interest.

References

1. M. P. DeLisa, Z. Zhang, M. Shiloach, S. Pilevar, C. C. Davis, J. S. Sirkis, and W. E. Bentley, "Evanescent wave long-period fiber Bragg grating as an immobilized antibody biosensor," Anal. Chem. 72 2895-2900 (2000).
2. D. Sun, T. Guo, Y. Ran, Y. Huang, and B. O. Guan, "In-situ DNA hybridization detection with a reflective microfiber grating biosensor," Biosens. Bioelectron. 61, 541-546 (2014).
3. S. Sridevi, K. S. Vasu, S. Asokan, and A. K. Sood, "Sensitive detection of C-reactive protein using optical fiber Bragg gratings," Biosens. Bioelectron. 65, 251-256 (2015).
4. B. Luo, S. Wu, Z. Zhang, W. Zou, S. Shi, M. Zhao, N. Zhong, Y. Liu, X. Zou, L. Wang, W. Chai, C. Hu, and L. Zhang, "Human heart failure biomarker immunosensor based on excessively tilted fiber gratings," Biomed. Opt. Express 8, 57-67 (2017).
5. W. Yu, T. Lang, J. Bian, and W. Kong, "Label-free fiber optic biosensor based on thin-core modal interferometer," Sensors & Actuators B Chemical 228, 322-329, (2016).
6. Z. Li, C. Liao, D. Chen, J. Song, W. Jin, G. D. Peng, F. Zhu, Y. Wang, J. He, and Y. P. Wang, "Label-free detection of bovine serum albumin based on an in-fiber Mach-Zehnder interferometric biosensor," Opt. Express 25(15), 17105-17113 (2017).
7. A. Mansaray, J. Rabah, M. Duran, and R. Wynne, "Human immunoglobulin class G (IgG) antibody detection with photonic crystal fiber," J. Lightwave Technol. 34, 1398-1404, (2016).
8. S. Chen, Y. Liu, Q. Liu, Z. Liu, and W. Peng, "Self-reference surface plasmon resonance biosensor based on multiple-beam interference," IEEE Sens. J. 16, 7568–7571 (2016).
9. R. Bharadwaj, S. Mukherji, and S. Mukherji, "Probing the localized surface plasmon field of a gold nanoparticle-based fibre optic biosensor, Plasmonics 11, 753-761 (2016).

Peer-reviewed version available at Micromachines 2020, 11, 270; doi:10.3390/mi11030270

10. C. Liu, Q. Cai, B. Xu, W. Zhu, L. Zhang, J. Zhao, X. Chen, “Graphene oxide functionalized long period grating for ultrasensitive label-free immunosensing,” Biosens. Bioelectron. 94(15), 200-206 (2017).
11. C. Liu, B. Xu, L. Zhou, Z. Sun, H. J. Mao, J. L. Zhao, L. Zhang, and X. Chen, “Graphene oxide functionalized long period fiber grating for highly sensitive hemoglobin detection,” Sensors & Actuators B Chemical 261, 91-96, 2018.
12. H. Luo, Q. Sun, X. Li, et al., “Refractive index sensitivity characteristics near the dispersion turning point of the multimode microfiber-based Mach-Zehnder interferometer,” Opt. Lett. 40(21), 5042-5 (2015).
13. K. Li, T. Zhang, G. Liu, et al., “Ultrasensitive optical microfiber coupler based sensors operating near the turning point of effective group index difference,” Appl. Phys. Lett. 109(10), 101101 (2016).
14. K. Li, M. Zhang, N. Zhang, et al., “Spectral characteristics and ultrahigh sensitivity near the dispersion turning point of optical microfiber couplers,” Journal of Lightwave Technology 36, 2409-2415 (2018).
15. W. Zhou, K. Li, Y. Wei, P. Hao, M. Chi, Y. Liu, and Y. Wu, “Ultrasensitive label-free optical microfiber coupler biosensor for detection of cardiac troponin I based on interference turning point effect,” Biosens. Bioelectron. 106, 99-104 (2018).
16. K. Li, N. Zhang, M. Zhang, G. Liu, T. Zhang, and L. Wei, “Ultrasensitive measurement of gas refractive index using an optical nanofiber coupler,” Opt. Lett. 43, 679-682 (2018)
17. W. Talataisong, R. Ismaeel, T. Lee, M. Beresna, and G. Brambilla, “Optical Nanofiber Coupler Sensors Operating in the Cut-Off Wavelength Region,” IEEE Sens. J 18(7), 2782-2787(2018).
18. Y. Jung, G. Brambilla, and D. J. Richardson, “Broadband single-mode operation of standard optical fibers by using a sub-wavelength optical wire filter,” Opt. Express 16(19), 14661-14667 (2008).
19. B. Sun, F. Fang, Z. Zhang, et al., “High-sensitivity and low-temperature magnetic field sensor based on tapered two-mode fiber interference,” Opt. Lett. 43(6), 1311-1314 (2018).
20. F. Fang, B. Sun, Z. Zhang, J. Xu, and L. Zhang, "Improvement on refractive index sensing by exploiting the tapered two-mode fibers," Chin. Opt. Lett. 17, 110604- (2019).